The evolution of spectral intensity and orbital angular momentum of twisted Hermite Gaussian Schell model beams in turbulence

RONG LIN,[1,2] **HANCHENG YU,**[1,3] **XINLEI ZHU,**[4] **LIN LIU,**[4] **GREG GBUR,**[5,6] **YANGJIAN CAI,**[1,3,4,7] **AND JIAYI YU**[1,3,8]

[1]*Shandong Provincial Engineering and Technical Center of Light Manipulations & Shandong Provincial Key Laboratory of Optics and Photonic Device, School of Physics and Electronics, Shandong Normal University, Jinan 250358, China*

[2]*College of Physics and Electronic Engineering, Heze University, Heze 274015, China*

[3]*Collaborative Innovation Center of Light Manipulations and Applications, Shandong Normal University, Jinan 250358, China*

[4]*School of Physical Science and Technology, Soochow University, Suzhou 215006, China*

[5]*Department of Physics and Optical Science, University of North Carolina at Charlotte, Charlotte, North Carolina 28223, USA*

[6]*gjgbur@uncc.edu*

[7]*yangjiancai@suda.edu.cn*

[8]*jiayiyu0528@sdnu.edu.cn*

Abstract: We introduce a new class of twisted partially coherent beams with a non-uniform correlation structure. These beams, called twisted Hermite Gaussian Schell model (THGSM) beams, have a correlation structure related to Hermite functions and a twist factor in their degree of coherence. The spectral density and total average orbital angular momentum per photon of these beams strongly depend on the distortions applied to their degree of coherence. On propagation through free space, they exhibit both self-splitting and rotation of their spectral density profile, combining the interesting effects of twisted beams and non-uniformly correlated beams. We demonstrate that we can adjust both the beam order and the twist factor of THGSM beams to improve their resistance to turbulence.

1.   Introduction

Beams carrying orbital angular momentum (OAM) have attracted a great deal of attention due to their many important applications, such as increasing the information capacity of optical communications [1], acting as a spanner to rotate microscopic particles [2], and detecting spinning objects [3]. It is well known that beams with a vortex phase possess OAM. However, partially coherent beams with a so-called twist phase also typically carry OAM [4,5], and this twist may be exploited in a manner similar to optical vortices.

The concept of a twist phase and the typical beams with twist phase, twisted Gaussian Schell model (TGSM) beams, were first introduced by Simon and Mukunda in 1993 [6], and were experimentally realized by Friberg et al. in 1994 [7]. The twist phase appears in the correlation function of a partially coherent beam (PCB), and is a function of two positions in the cross-section of the beam. This phase cannot be separated into a product of simpler one-dimensional contributions, which differs from the quadratic phase factors associated with spreading and focusing of a beam. The twist phase can therefore only exist in partially coherent beams: the magnitude of the phase is bounded from above by the inverse square of the transverse coherence width, and it vanishes in the limit of full coherence [6]. In addition, this phase displays handedness and results in the rotation of the beam spot on propagation [6–8]. Because of its unique characteristics, researchers have focused great attention on PCBs with a twist phase and

have found that they have many useful applications, such as improving the performance of ghost imaging [9], overcoming the classical Rayleigh limit in imaging [10], and resisting detrimental turbulence-induced effects [11]. However, most of studies have been limited to TGSM beams, due to the difficulty in embedding the twist phase into PCBs with a more complicated correlation structure.

However, after a new method for designing novel correlation structures for scalar and vector PCBs was introduced by Gori and his co-workers [12,13], much effort has focused on PCBs with a prescribed correlation structure and their extraordinary properties. For example, partially coherent non-uniformly correlated beams display self-focusing properties [14,15], Hermite Gaussian Schell model beams exhibit self-splitting properties [16], and Laguerre Gaussian correlated Schell model beams possess ring-shaped intensity profiles in the far field [17]. Furthermore, all the beams mentioned above display excellent resistance to turbulence, i.e., they reduce scintillation, beam wander, beam spreading and other negative effects which reduce the reliability of laser radar, remote sensing systems and free-space optical communications [18–21].

As both twisted beams and non-uniformly correlated beams possess potentially beneficial characteristics, both in free space and turbulence, it is natural to investigate whether these characteristics can be combined in a single beam. In this paper, we introduce a class of twisted PCBs with a prescribed correlation structure that we call twisted Hermite Gaussian Schell model (THGSM) beams. The DOC of these beams is non-uniformly correlated and possesses a twist factor. The propagation properties of such beams are studied in free space and in atmospheric turbulence, and it is shown that one can adjust the beam order and twist factor to enhance the total OAM of the beams and, simultaneously, improve their resistance to turbulence. With multiple degrees of freedom that can be adjusted to optimize the beam for different turbulence conditions, THGSM beams are an excellent candidate for use in optical applications in challenging media.

2. Theoretical model for THGSM beams

Typically, the spatial coherence properties of scalar PCBs are described by the cross-spectral density (CSD) function in the space-frequency domain and by the mutual coherence function in the space-time domain. Both of these functions have to be nonnegative definite kernels. In recent years, the CSD function has become the quantity of choice for studying quasi-monochromatic fields, and it is defined as a two-point correlation function at the source plane:

$$W\left(\mathbf{r}_1, \mathbf{r}_2\right) = \left\langle E^*\left(\mathbf{r}_1\right) E\left(\mathbf{r}_2\right)\right\rangle_\omega, \tag{1}$$

where $E(\mathbf{r})$ denotes the electric field fluctuating in a direction transverse to the z-axis, and the angular brackets $\langle \quad \rangle_\omega$ means an average over a ensemble of monochromatic field realizations. The asterisk indicates the complex conjugate, and the quantities $\mathbf{r}_1$ and $\mathbf{r}_2$ are two arbitrary position vectors in the transverse plane. To be a mathematically genuine correlation function, the CSD must correspond to a nonnegative definite kernel, which is fulfilled if the function can be written in the following form [12]

$$W\left(\mathbf{r}_1, \mathbf{r}_2\right) = \int p\left(\mathbf{v}\right) V_0^*\left(\mathbf{r}_1, \mathbf{v}\right) V_0\left(\mathbf{r}_2, \mathbf{v}\right) d^2\mathbf{v}, \tag{2}$$

where $p(\mathbf{v})$ is a non-negative function and $V_0(\mathbf{r}, \mathbf{v})$ is an arbitrary kernel.

A vast amount of research has shown that different choices for $p(\mathbf{v})$ and $V_0(\mathbf{r}, \mathbf{v})$ can generate very different kinds of PCBs with distinct behaviors [22]. Here, we choose these functions to combine unusual behaviors of two classes of beams studied previously. To produce a

Hermite-correlated beam, we choose $p(\mathbf{v})$ in the form [15],

$$p(\mathbf{v}) = (1/4\pi)(4a)^{2m+1}(v_x v_y)^{2m} \exp\left(-a\mathbf{v}^2\right), \qquad (3)$$

where m is the beam order. With a chosen as a positive real constant, $p(\mathbf{v})$ is a non-negative function, resulting in a mathematically valid CSD. To give the beam a twist phase, we set V_0 as [23]

$$V_0(\mathbf{r}, \mathbf{v}) = \exp\left(-\sigma \mathbf{r}^2\right) \exp\left\{-\left[(auy + ix)v_x - (aux - iy)v_y\right]\right\}. \qquad (4)$$

The quantity σ is a positive real constant characterizing the width of the kernel function, a is a positive real constant that determines the coherence width, and u is a real constant representing the twist factor.

Substituting Eqs. (3) and (4) into Eq. (2), a lengthy but straightforward calculation results in the following expression for the CSD function,

$$
\begin{aligned}
W(\mathbf{r}_1, \mathbf{r}_2) ={}& \exp\left(-\frac{\mathbf{r}_1^2 + \mathbf{r}_2^2}{4\omega_0^2}\right) \exp\left[-\frac{(\mathbf{r}_1 - \mathbf{r}_2)^2}{2\delta_g^2}\right] \exp\left[-iu(x_1 y_2 - x_2 y_1)\right] \\
& \times H_{2m}\left[\frac{1}{2\sqrt{a}}(x_1 - x_2) + \frac{iu\sqrt{a}}{2}(y_1 + y_2)\right] H_{2m}\left[\frac{1}{2\sqrt{a}}(y_1 - y_2) - \frac{iu\sqrt{a}}{2}(x_1 + x_2)\right],
\end{aligned}
$$
$$(5)$$

where $\omega_0 = \left(4\sigma - 2au^2\right)^{-1/2}$ is the beam width parameter, $\delta_g = \sqrt{2}\left(1/a + au^2\right)^{-1/2}$ is the coherence width parameter and $H_{2m}(x)$ denotes the Hermite polynomial of order $2m$.

In typical studies of twisted beams, e.g. Reference [6], an inequality relating the coherence width δ_g and the twist factor u is provided, as not every choice of these parameters represents a physically realizable beam. In our derivation using Eq. (2), however, we begin with a physically realizable beam and derive the form of the cross-spectral density. The result is a beam which is valid for all twist parameters u, but with δ_g itself a function of u.

Equation (5) shows that the CSD function of this new class of beams contains a twist term as well as correlations based on Hermite polynomials; thus we refer to these beams as THGSM beams. For the case $m = 0$ and $u \neq 0$, THGSM beams reduce to a TGSM form; for the case $m > 0$ and $u = 0$, THGSM beams reduce to a Hermite-Gaussian correlated Schell-model (HGCSM) beam [16]. In the special case $m = 0$ and $u = 0$, THGSM beams reduce to a conventional Gaussian Schell model form. THGSM beams therefore serve as a superset that includes the preceding types as limiting cases.

It is to be noted that Eq. (5) is not strictly of Schell model form. The arguments of the Hermite functions and the twist phase are not Schell model. However, TGSM beams themselves are not strictly Schell model due to the twist phase, so we refer to our THGSM beams as Gaussian Schell model due to the presence of the Gaussian term that depends only on $(\mathbf{r}_1 - \mathbf{r}_2)^2$.

Two standard quantities of interest in the study of PCBs are the spectral density $S(\mathbf{r})$ and the degree of coherence $\mu(\mathbf{r}_1, \mathbf{r}_2)$. By setting $\mathbf{r}_1 = \mathbf{r}_2 = \mathbf{r}$, the CSD function reduces to the spectral density function. The DOC is given by the expression,

$$\mu(\mathbf{r}_1, \mathbf{r}_2) = \frac{W(\mathbf{r}_1, \mathbf{r}_2)}{\sqrt{W(\mathbf{r}_1, \mathbf{r}_1)\, W(\mathbf{r}_2, \mathbf{r}_2)}}. \qquad (6)$$

Similar expressions apply for the spectral density and DOC at any propagation distance z.

Figure 1 shows the density plot of the absolute value of the DOC of the proposed THGSM beams for different values of the beam order m and twist factor u in the source plane. One confirms from comparing Figs. 1(a1) and 1(b1) that the number of side lobes increases as the beam order m increases. Comparing Figs. 1(a1)–1(a3) or Figs. 1(b1)–1(b3), we note that the twist factor distorts the DOC much more dramatically with increasing u.
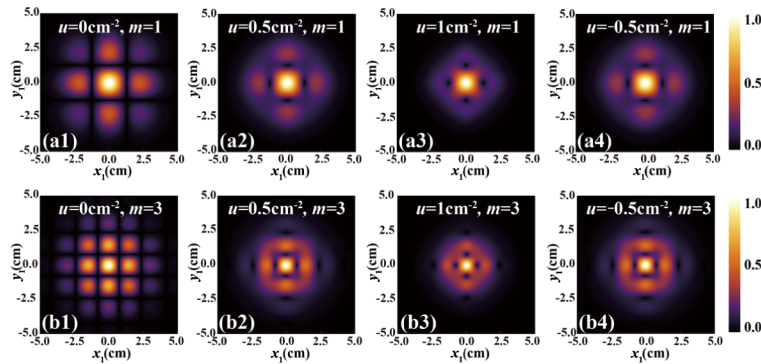
Fig. 1. Density plot of the absolute value of the DOC of THGSM beams for different values of the beam order m and twist factor u. The position vector $\mathbf{r}_2 = 0$ and the DOC is plotted as a function of (x_1, y_1).

The corresponding spectral intensity distributions of the beams are plotted in Fig. 2. We find the beam profile gradually splits from one Gaussian beam spot to four spots; furthermore, the value of the beam order also affects the degree of splitting. It should be noted, from the second and fourth columns in the Fig. 1 and Fig. 2, that the distribution of the spectral density and the DOC are independent of the sign (or the handedness) of the twist factor.
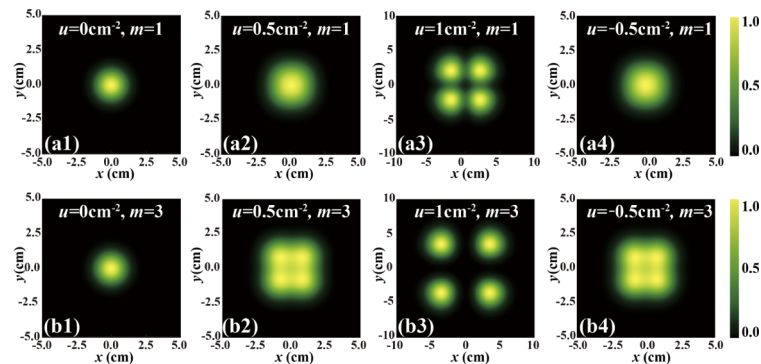
Fig. 2. Density plot of the normalized intensity of THGSM beams for different values of the beam order m and twist factor u.

The twist factor dependence of these beams is quite different from conventional TGSM beams, which keep the same Gaussian beam profile regardless of the choice of twist factor [6,7]. However, the spectral density of our THGSM beams is modulated by the Hermite function which depends on both the beam order and twist factor. We therefore have a class of twisted partially coherent beams with distinct correlation functions.

3. The CSD and OAM of THGSM beams propagation in turbulence

Beams with OAM and/or partial coherence have been viewed as key in improving free-space optical communication through atmospheric turbulence; THGSM beams possess both characteristics simultaneously. In this section, the CSD and OAM of THGSM beams propagating in free space and turbulent atmosphere are derived. In the following section we study their propagation characteristics.

Paraxial propagation of the CSD of PCBs in turbulence can be treated by the generalized Huygens-Fresnel integral [24],

$$W(\boldsymbol{\rho}_1, \boldsymbol{\rho}_2, z) = \left(\frac{k}{2\pi z}\right)^2 \int \int_{-\infty}^{\infty} W(\mathbf{r}_1, \mathbf{r}_2) \exp\left[-\frac{ik}{2z}(\mathbf{r}_1 - \boldsymbol{\rho}_1)^2 + \frac{ik}{2z}(\mathbf{r}_2 - \boldsymbol{\rho}_2)^2\right]$$
$$\times \langle \exp\left[\Psi(\mathbf{r}_1, \boldsymbol{\rho}_1) + \Psi^*(\mathbf{r}_2, \boldsymbol{\rho}_2)\right]\rangle d^2\mathbf{r}_1 d^2\mathbf{r}_2, \tag{7}$$

where $\boldsymbol{\rho}_1 \equiv (\rho_{1x}, \rho_{1y})$ and $\boldsymbol{\rho}_2 \equiv (\rho_{2x}, \rho_{2y})$ represent two arbitrary transverse position vectors at the receiver plane, $k = 2\pi/\lambda$ is wave number, with λ being the wavelength, and Ψ denotes the complex phase perturbation induced by the refractive-index fluctuations of the random medium between source position $\mathbf{r}$ and detector position $\boldsymbol{\rho}$. The ensemble average term in Eq. (7) can be expressed as [15,18]

$$\langle \exp\left[\Psi(\mathbf{r}_1, \boldsymbol{\rho}_1) + \Psi^*(\mathbf{r}_2, \boldsymbol{\rho}_2)\right]\rangle$$
$$= \exp\left\{-\left(\frac{\pi^2 k^2 z}{3}\right)\left[(\boldsymbol{\rho}_1 - \boldsymbol{\rho}_2)^2 + (\boldsymbol{\rho}_1 - \boldsymbol{\rho}_2)\cdot(\mathbf{r}_1 - \mathbf{r}_2) + (\mathbf{r}_1 - \mathbf{r}_2)^2\right]\int_0^{\infty} \kappa^3 \Phi_n(\kappa) d^2\kappa\right\}, \tag{8}$$

where $\Phi_n(\kappa)$ is the spatial power spectrum of the refractive-index fluctuations of the turbulent atmosphere. For brevity, we set

$$T = \int_0^{\infty} \kappa^3 \Phi_n(\kappa) d^2\kappa. \tag{9}$$

We model the turbulence using the van Karman power spectrum, which can describe Kolmogorov ($\alpha = 11/3$) and non-Kolmogorov ($\alpha \neq 11/3$) power spectrum; for this model T can be expressed in the form,

$$T = \frac{\Omega(\alpha)}{2(\alpha - 2)} C_n^2 \left[\beta \kappa_m^{2-\alpha} \exp\left(\kappa_0^2/\kappa_m^2\right) \Gamma_1\left(2 - \alpha/2, \kappa_0^2/\kappa_m^2\right) - 2\kappa_0^{4-\alpha}\right], 3 < \alpha < 4, \tag{10}$$

where $\Omega(\alpha) = \Gamma(\alpha - 1)\cos(\alpha\pi/2)/4\pi^2$, and $\Gamma(\cdot)$ represents the Gamma function. C_n^2 is a generalized refractive-index structure parameter with units $\text{m}^{3-\alpha}$, $\beta = 2\kappa_0^2 - 2\kappa_m^2 + \alpha\kappa_m^2$ and $\Gamma_1(\cdot)$ is the incomplete Gamma function. Other turbulence-dependent parameters are $\kappa_0 = 2\pi/L_0$, with L_0 being the outer scale of turbulence, and $\kappa_m = c(\alpha)/l_0$, with $c(\alpha) = [2\pi\Omega(\alpha)\Gamma(5 - \alpha/2)/3]^{1/(\alpha-5)}$ and l_0 being the inner scale of turbulence.

By inserting our expression for a THGSM beam, Eq. (5), into Eq. (7), and performing some tedious integration, we obtain the expression of the CSD function of THGSM beams in the target plane after passing through turbulence,

$$W(\boldsymbol{\rho}_1, \boldsymbol{\rho}_2, z) = C_0 \exp\left[\frac{ik}{2z}\left(\rho_2^2 - \rho_1^2\right) - T'(\boldsymbol{\rho}_1 - \boldsymbol{\rho}_2)^2 + \frac{1}{4A_1}\left(\frac{ik}{z}\boldsymbol{\rho}_1 - T'(\boldsymbol{\rho}_1 - \boldsymbol{\rho}_2)\right)^2\right]$$
$$\times \exp\left\{\frac{1}{4A_2}\left[\frac{ik}{z}\left(\frac{T'}{A_1}\boldsymbol{\rho}_1 - \boldsymbol{\rho}_2\right) + T'\left(1 - \frac{T'}{A_1}\right)(\boldsymbol{\rho}_1 - \boldsymbol{\rho}_2)\right]^2 + \frac{1}{J}\left(G_+^2 + G_-^2\right)\right\}, \tag{11}$$

The parameters in Eq. (11) have a complicated dependence on position and are given as follows,

$$A_1 = \sigma + \frac{ik}{2z} + T', \quad A_2 = \sigma - \frac{ik}{2z} + T' - \frac{T'^2}{4A_1}, \quad T' = \frac{\pi^2 k^2 z T}{3}, \tag{12a}$$

$$J = -\left(\frac{T'}{2A_1 A_2} - \frac{1}{4A_2}\right)\left(a^2 u^2 + 1\right) - \left(\frac{T'^2}{4A_1^2 A_2} + \frac{1}{4A_1}\right)\left(a^2 u^2 - 1\right)\frac{1}{2A_2}a^2 u^2 + a, \tag{12b}$$

$$G_{\pm} = \frac{1}{4A_1}\left(\frac{k}{z} + iT'\right)\left(\pm iau\rho_{1x} - \rho_{1y}\right) - \frac{iT'}{4A_1}\left(\pm iau\rho_{2x} - \rho_{2y}\right)$$

$$+ \frac{1}{4A_2}\left[\pm\frac{iauk}{z}\left(\frac{T'^2}{A_1^2}\rho_{1x} - \rho_{2x}\right) - \frac{k}{z}\left(\frac{T'}{A_1} - 1\right)\left(\frac{T'}{A_1}\rho_{1y} - \rho_{2y}\right)\right] \quad (12c)$$

$$+ \frac{1}{4A_2}\left[\pm auT'\left(\frac{ik}{A_1 z} - \frac{T'^2}{A_1^2} + 1\right)(\rho_{1x} - \rho_{2x}) - iT'\left(\frac{T'}{A_1} - 1\right)^2(\rho_{1y} - \rho_{2y})\right],$$

$$C_0 = \sum_{l=0}^{m}\sum_{d=0}^{m}\frac{4^{2m-l-d-1}a^{2m+1}k^2(2m)!(2m)!G_{+}^{2m-2l}G_{-}^{2m-2d}}{d!l!z^2 A_1 A_2(2m-2l)!(2m-2d)!J^{4m-d-l+1}}. \quad (12d)$$

For Eq. (12c), when the sign is "+", the subscript of the coordinate stays the same i.e., $x = x$ and $y = y$; when the sign is "-", the subscripts of the coordinates are swapped i.e., $x = y$ and $y = x$.

The spectral density (or intensity) in the output plane is obtained simply as

$$S(\boldsymbol{\rho}, z) = W(\boldsymbol{\rho}, \boldsymbol{\rho}, z). \quad (13)$$

Because of the twist phase, we expect THGSM beams to possess non-zero OAM. For paraxial scalar PCBs, the OAM flux density along the z axis may be written using the cross-spectral density as [25,27]

$$O(\boldsymbol{\rho}, z) = -\frac{\varepsilon_0}{k}\text{Im}\left[\rho_{1y}\partial_{\boldsymbol{\rho}_{2x}}W(\boldsymbol{\rho}_1, \boldsymbol{\rho}_2, z) - \rho_{1x}\partial_{\boldsymbol{\rho}_{2y}}W(\boldsymbol{\rho}_1, \boldsymbol{\rho}_2, z)\right]_{\boldsymbol{\rho}_1=\boldsymbol{\rho}_2=\boldsymbol{\rho}}, \quad (14)$$

where $\partial_{\boldsymbol{\rho}_{2x}}$ and $\partial_{\boldsymbol{\rho}_{2y}}$ denote partial derivatives with respect to $\boldsymbol{\rho}_{2x}$ and $\boldsymbol{\rho}_{2y}$, and ε_0 denotes the free-space permittivity.

The OAM flux density indicates the spatial distribution of OAM in a transverse plane of the beam. This quantity depends not only on the strength of circulation of the beam at a point, however, but also the beam intensity. To better understand how OAM is distributed throughout the beam's cross-section, we define the normalized OAM flux density and the total average OAM per photon, respectively, as

$$O_n(\boldsymbol{\rho}, z) = \frac{\hbar\omega O(\boldsymbol{\rho}, z)}{S_p(\boldsymbol{\rho}, z)}, \quad (15)$$

$$O_t(\boldsymbol{\rho}, z) = \frac{\hbar\omega\int O(\boldsymbol{\rho}, z)d^2\boldsymbol{\rho}}{\int S_p(\boldsymbol{\rho}, z)d^2\boldsymbol{\rho}}, \quad (16)$$

where $\hbar$ is Planck constant divided by 2π and $S_p(\boldsymbol{\rho}, z)$ is the z component of the Poynting vector, which is of the form

$$S_p(\boldsymbol{\rho}, z) = \frac{k}{\mu_0\omega}W(\boldsymbol{\rho}, \boldsymbol{\rho}, z), \quad (17)$$

where μ_0 is vacuum permeability. Equation (16) provides the total OAM per photon in the cross-section of the beam, while Eq. (16) describes the average OAM per photon at a particular point in the beam's cross-section. Substituting from Eq. (11) into Eqs. (15) and (16), we can derive expressions for the normalized OAM flux and the total average OAM per photon of THGSM beams and determine how they change on propagation through the atmosphere.

## 4. The CSD and OAM of THGSM beams propagating in free space and in turbulence

In this section, we study the propagation properties of THGSM beams propagating in free space ($C_n^2 = 0$) and in a turbulent atmosphere by using the formulas derived above. In the following numerical examples, the parameters of the beams and the turbulence are set as $\lambda = 632.8$nm,

$\sigma = 0.5\text{cm}^{-2}$, $a = 0.8\text{cm}^2$, $C_n^2 = 5 \times 10^{-15}\text{m}^{-2/3}$, $L_0 = 1\text{m}$, $l_0 = 1\text{mm}$. These values are representative of those often used in laboratory tests of structured light beams. For the case of free space, we investigate how the Hermite and twist properties of the beam influence its propagation, and evaluate the dependence of OAM on these properties. For the case of turbulence, we study investigate how the random medium modifies the inherent beam characteristics.

4.1. In free space

Figure 3 shows the evolution of the normalized spectral density of THGSM beams propagating in free space with different values of beam order m and twist factor u. Figure 3(a) presents a beam with $m = 1$ and $u = 0$ (i.e., Hermite Gaussian Schell model beams) exhibiting self-splitting during propagation, showing that the behavior seen in Ref. [28] is maintained for our new beam class. Comparing Figs. 3(a) and 3(b), we see that a THGSM beam rotates with respect to its central axis on propagation as it splits, as expected for beams possessing a twist phase [23]. These beams therefore simultaneously display the effects associated with twisted beams and Hermite Gaussian Schell model beams.
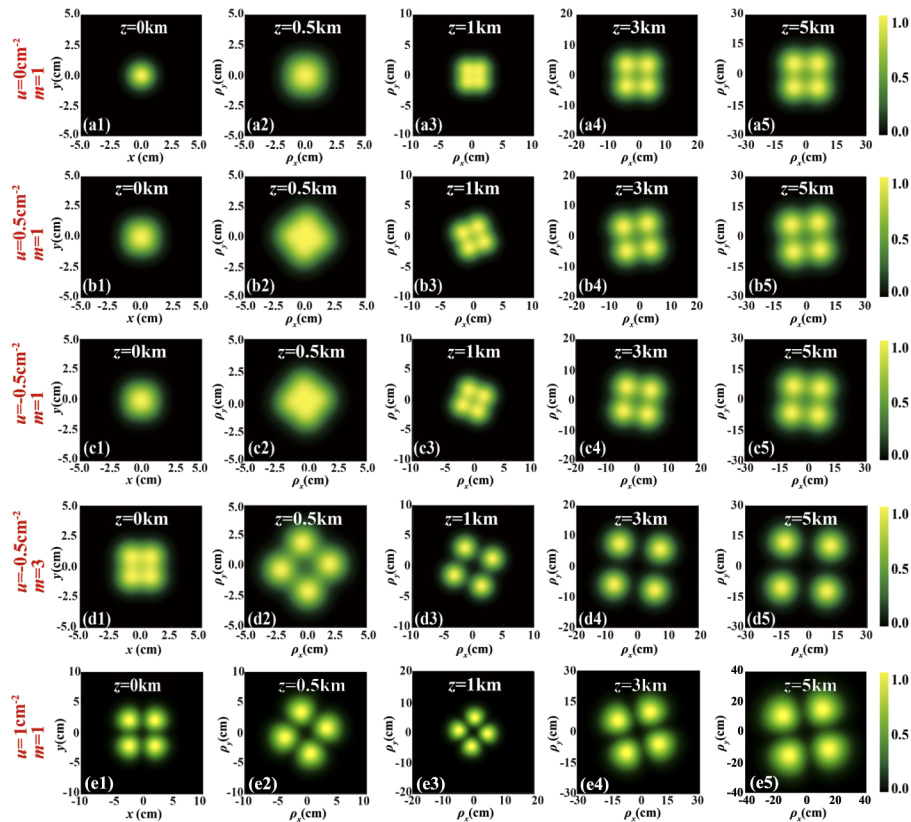

Fig. 3. Density plot of the normalized intensity of THGSM beams upon propagation in free space for different beam orders m and twist factors u.

One sees in Figs. 3(b) and 3(c) that the sign of the twist factor determines the rotation direction of the beam spot; the positive/negative value of u corresponds to clockwise/anti-clockwise rotation, based on the direction of light propagation. We confirm from comparing Figs. 3(b) and 3(e) that THGSM beams with larger twist factor will split much deeply and continue rotating over longer propagation distances. Figure 3(d) shows a beam with a larger order ($m = 3$), and

one finds that the beam splits even more, which indicates beam order can be used to control the degree of splitting.

One of the most significant characteristics of THGSM beams is an orbital angular momentum that can be tuned using several beam parameters. Figure 4(a) shows the total average OAM per photon of the beams with different beam order m on propagation in free space; the figure verifies the conservation of total OAM. It is to be noted that the value of the total average OAM per photon increases with beam order, even though the twist factor remains the same, and even though there is no underlying vortex structure associated with the beam order in Eq. (4).
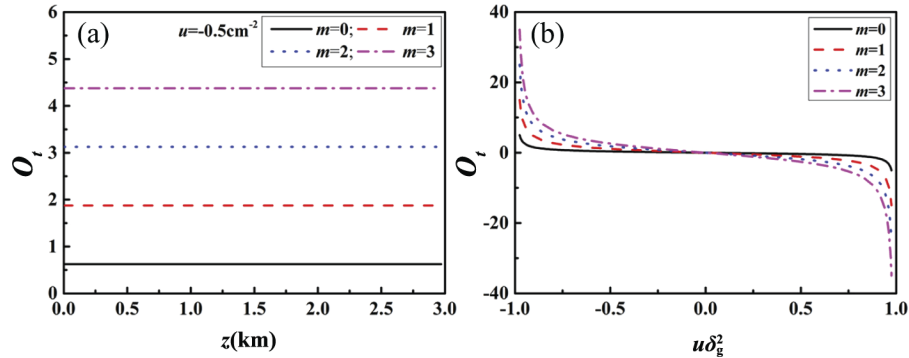

Fig. 4. The total average OAM per photon of THGSM beams with different beam order m versus (a) the transmission distance in free space; (b) the normalized factor $u\delta_g^2$ in the source plane.

Figure 4(b) further illustrates how the total average OAM per photon depends on the beam parameters. It can be seen that the direction of the total average OAM per photon is only determined by the sign of the twist factor. For the negative value of u, the handedness of the total average OAM per photon is along the propagation direction, causing the beam spot to rotate in the anti-clockwise direction as it travels. When the value of u is positive, the situation is reversed. Figure 4(b) shows that the total average OAM per photon increases with increasing beam order and larger twist factor. Thus, THGSM beams have two free parameters for controlling the total average OAM per photon: the twist factor and the beam order.

In recent years, researchers have also started focusing on the distribution of OAM in the beam cross-section, as it gives a picture of the nature of the beam's circulation [26]. It has been shown [25] that traditional TGSM beams possess a normalized OAM flux density that increases quadratically with radial distance, making them behave like rigid-body rotators. Figure 5(a) shows the normalized OAM flux density of THGSM beams for different beam orders. We can now see that THGSM beams also have a quadratic normalized OAM flux density, and that this flux density increases with increasing beam order. Figure 5(b) shows how the normalized OAM flux density of the beams changes as the beam propagates. The OAM flux density is calculated at point (2cm, 2cm) versus the propagation distance in free space; the quantitative behavior of the figure will change if this observation point is changed, but not the qualitative evolution. The value of the normalized OAM flux density decreases gradually on propagation, and beams with larger beam order always have larger normalized OAM flux density, although it decreases sharply over short propagation distance. This decrease is evidently associated with the splitting property of the beam, which redistributes the OAM to larger radial distances.
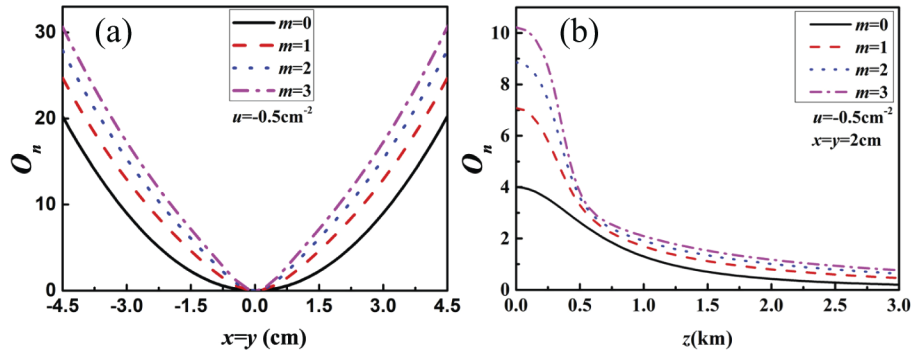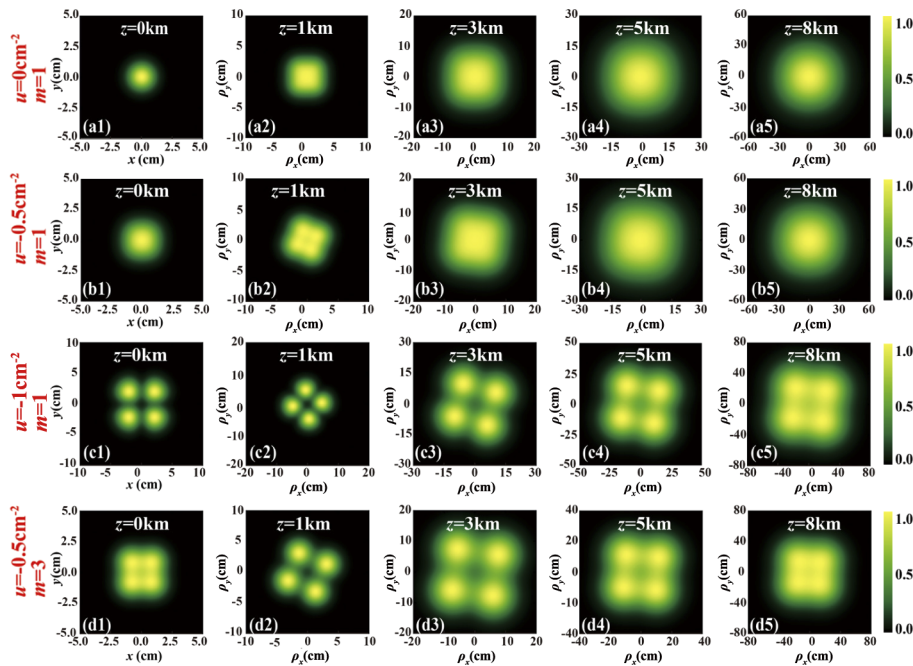
Fig. 5. The normalized OAM flux density of THGSM beams with different beam order *m* versus (a) position coordinates in the source plane; (b) propagation distance at point (2cm, 2cm) in free space.

4.2. In turbulent atmosphere

The use of partially coherent beams and OAM beams in turbulence has proven useful for a number of applications. Here we investigate how the characteristics of THGSM beams are changed when they propagate in the atmosphere.

Figure 6 shows the distribution of the normalized intensity of THGSM beams at different distances in turbulence with different beam order *m* and twist factor *u*, to be compared with Fig. 3. It can be seen that THGSM beams still undergo self-splitting and rotation even in turbulence. Figure 6 also shows that the beam profile of THGSM beams inevitably evolves to a Gaussian profile over long propagation distances; this behavior is attributable to the accumulated influence

Fig. 6. Density plot of the normalized intensity of THGSM beams upon propagation in turbulence for different beam order *m* and twist factor *u*.

of the spatially isotropic turbulence. Comparing Figs. 6(a)–6(c), one finds that the evolution of the intensity is strongly affected by the twist factor u; a beam with larger u can maintain its split profile over a longer distance than a beam with small u; this indicates that THGSM beams possessing a twist phase are less affected by turbulence. We see from Figs. 6(b) and 6(d) that a THGSM beam with larger beam order can also maintain its split profile over a longer propagation distance than a THGSM beam with small beam order. Evidently, beams with a higher order are more resistant to turbulence degradation.

We may characterize the splitting property of THGSM beams by calculating the ratio of the spectral intensity on the optical axis ($\rho = 0$) to the maximum spectral intensity in the transverse plane of THGSM beams; a low axial intensity corresponds to significant splitting. Figure 7 plots this ratio versus the propagation distance in turbulence for different values of the beam order m and the twist factor u. One sees from Fig. 7 that the value of the ratio decreases relatively quickly over short propagation distances, illustrating the splitting of the original single beam spot into four beam spots. The ratio increases to one at long propagation distances, which shows that the four beam spots degrade and combine to one beam spot (Gaussian distribution). Furthermore, the ratio of the spectral intensity of THGSM beams with larger beam order m and twist factor u degrades slower than that of the beams with smaller parameters. These results again indicate that THGSM beams with larger beam order m and twist factor u are less affected by turbulence.
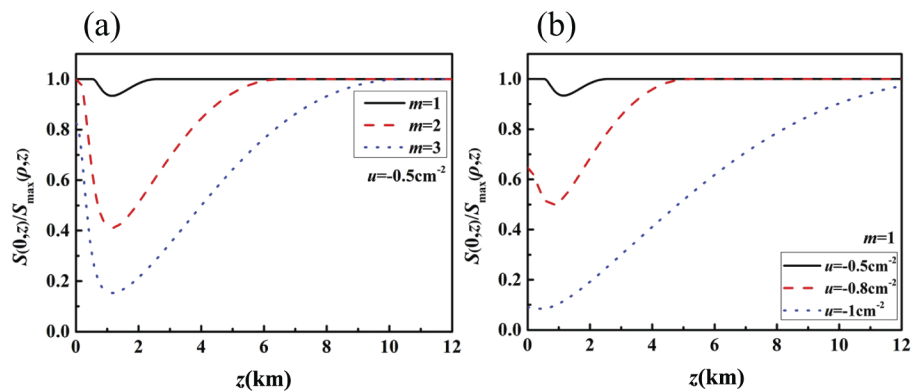

Fig. 7. Ratio $S(0, z)/S_{\max}(\rho, z)$ of the spectral intensity in the optical axis to the maximum intensity in the transverse plane of THGSM beams with different (a) twist factor and (b) beam order on propagation.

We next consider the influence of turbulence on the OAM of THGSM beams. Figure 8(a) shows the total average OAM per photon of the beams with different beam order m on propagation in turbulence. We find that the total average OAM per photon of the beams remains invariant on propagation in turbulence. This is to be expected because the turbulence is isotropic: though OAM may be lost or gained on propagation through any particular realization of the turbulent medium, on average these fluctuations average to zero. Figure 8(b) shows the total average OAM per photon of THGSM beams with different beam order m versus the normalized factor $u\delta_g^2$ at $z = 1$km in turbulence. This figure is essentially identical to Fig. 4(b); it again shows that the value of the total average OAM per photon increases with larger beam order and twist factor.

Figure 9(a) shows the normalized OAM flux density of THGSM beams with different beam order m on propagation in turbulence, again using a reference point $(2\text{cm}, 2\text{cm})$. We find the value of the normalized OAM flux density decreases gradually on propagation, as in free space. However, if we compare the spectral density for free space and turbulence propagation, Figs. 3 and 6, we see that the beam shapes are already significantly distorted at 3 km; the normalized OAM flux density plots of Figs. 5(b) and 9(a) are nevertheless quite similar over this range.
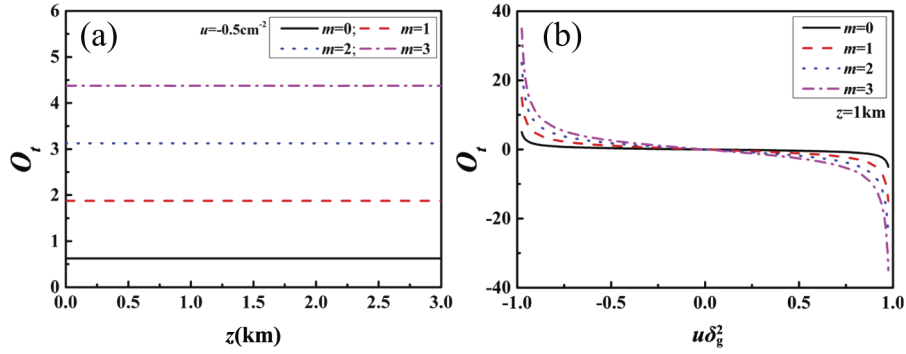
Fig. 8. The total average OAM per photon of THGSM beams with different beam order m versus (a) the transmission distance; (b) the normalized factor $u\delta_g^2$ at $z = 1$km in turbulence.
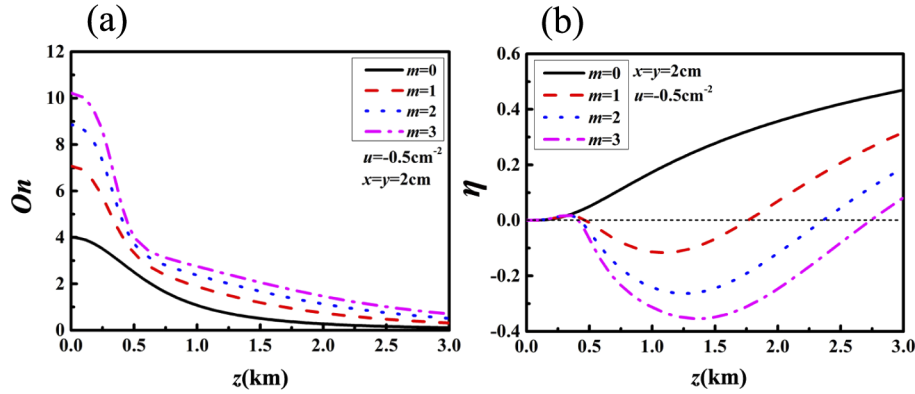
Fig. 9. The normalized OAM flux density of THGSM beams with different beam order m on propagation in turbulence at point $(2\text{cm}, 2\text{cm})$; (b) Degradation rate of the normalized OAM flux density in turbulence with different beam order m.

To better see the differences at the end of this propagation range, Fig. 9(b) compares the normalized OAM flux density in turbulence to that in free space for different beam orders. Here, we define a degradation rate of the THGSM beam in turbulence as follows,

$$\eta = \frac{O_{nfree} - O_{ntur}}{O_{nfree}} \times 100\%, \tag{18}$$

where O_{nfree} and O_{ntur} represent the normalized OAM flux density of THGSM beams in free space and in turbulence, respectively.

Figure 9(b) shows that the value of the degradation rate increases over short propagation distances, then it decreases to a minimum, after which it increases gradually. It is to be noted that the value of η becomes less than zero about $z = 500$m, which means the normalized OAM flux density of THGSM beams in turbulence is larger than that in free space at the point $(2\text{cm}, 2\text{cm})$. One can explain this phenomenon by the fact that the turbulence causes the four spot distribution of intensity of THGSM beams to merge into one uniform spot. Due to the accumulated influence of turbulence and the "dissipation" of light intensity as the propagation distance increases, the value of the degradation rate recovers to a positive value. Comparing the evolution of the degradation rate for different beam orders, we find that THGSM beams with a large beam order can keep the the normalized OAM flux density at one point much better, which again means that beams with larger beam order are less affected by turbulence.

Figure 10, which shows the normalized OAM flux density in free space and turbulence at 3 km, provides more insight into the effects of turbulence. It can be seen that, compared to the free space case, the beam in turbulence has had its quadratic behavior broadened. In essence, the OAM flux has been pushed further from the beam axis. Nevertheless, the higher-order beams maintain a higher OAM flux density near the core than the lower-order beams.
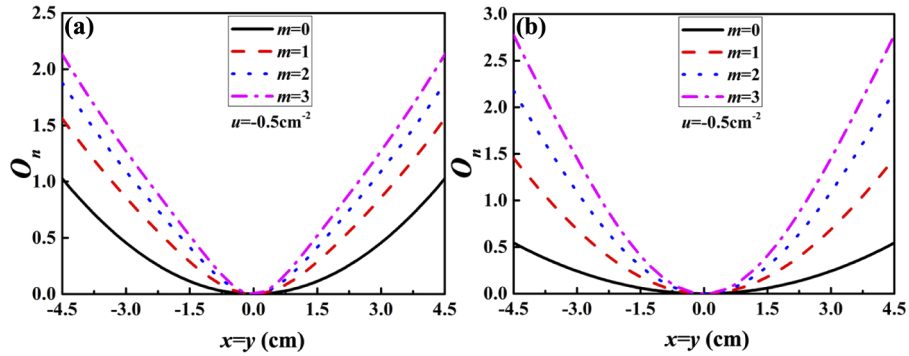
Fig. 10. The normalized OAM flux density of THGSM beams with different beam order m on propagation in (a) free space, and (b) in turbulence, at a propagation distance of 3 km.

Overall, we find that the average OAM of THGSM beams are, as expected, unchanged by turbulence, but the normalized OAM flux density is significantly broadened.

5. Summary

In this work, we have introduced a new class of twisted PCBs with a prescribed correlated structure, which we have labeled THGSM beams. These beams combine the characteristics of twisted beams and non-uniformly correlated beams, which have previously only been implemented in separate beam classes. In the source plane, we found that both the DOC and the spectral density are strongly influenced by the twist phase and beam order, resulting in non-uniform distributions. The total OAM of the beams is influenced by both of these parameters, giving us two means of controlling OAM in THGSM beams.

We have also studied the evolution of THGSM beams in free space and in turbulence, using analytic expressions for the cross-spectral density. Our results show that THGSM beams simultaneously possess the self-splitting and rotation properties of Hermite beams and twisted beams, respectively, and maintain these characteristics on propagation through turbulence. Furthermore, it was demonstrated that beams with higher order and twist factor are more resistant to turbulence.

It is to be noted that although higher-order beams have higher OAM and maintain their OAM flux density profile over longer propagation distances than lower-order beams, they also have lower on-axis intensity over much of their propagation distance, due to their self-splitting property. We therefore note that the optimal choice of beam for a specific application will likely involve a tradeoff between desired OAM characteristics and intensity characteristics. Overall, however, the broad class of THGSM beams perform significantly better than their less structured counterparts such as TGSM, HGCSM, and GSM beams.

THGSM beams therefore provide a significant degree of flexibility in the control of OAM and in providing improved resistance to turbulence.

Funding

Disclosures

The authors declare no conflicts of interest.

References

1. J. Wang, J. Yang, I. M. Fazal, N. Ahmed, Y. Yan, H. Huang, Y. Ren, Y. Yue, S. Dolinar, M. Tur, and A. E. Willner, "Terabit free-space data transmission employing orbital angular momentum multiplexing," Nat. Photonics **6**(7), 488–496 (2012).
2. D. G. Grier, "A revolution in optical manipulation," Nature **424**(6950), 810–816 (2003).
3. M. P. J. Lavery, F. C. Speirits, S. M. Barnett, and M. J. Padgett, "Detection of a spinning object using light's orbital angular momentum," Science **341**(6145), 537–540 (2013).
4. J. Serna and J. M. Movilla, "Orbital angular momentum of partially coherent beams," Opt. Lett. **26**(7), 405–407 (2001).
5. X. Peng, L. Liu, F. Wang, S. Popov, and Y. Cai, "Twisted Laguerre-Gaussian Schell-model beam and its orbital angular moment," Opt. Express **26**(26), 33956–33969 (2018).
6. R. Simon and N. Mukunda, "Twisted Gaussian Schell-model beams," J. Opt. Soc. Am. A **10**(1), 95–109 (1993).
7. A. T. Friberg, E. Tervonen, and J. Turunen, "Interpretation and experimental demonstration of twisted Gaussian Schell-model beams," J. Opt. Soc. Am. A **11**(6), 1818–1826 (1994).
8. H. Wang, X. Peng, L. Liu, F. Wang, Y. Cai, and S. A. Ponomarenko, "Generating bona fide twisted Gaussian Schell-model beams," Opt. Lett. **44**(15), 3709–3712 (2019).
9. Y. Cai, Q. Lin, and O. Korotkova, "Ghost imaging with twisted Gaussian Schell-model beam," Opt. Express **17**(4), 2453–2464 (2009).
10. Z. Tong and O. Korotkova, "Beyond the classical Rayleigh limit with twisted light," Opt. Lett. **37**(13), 2595–2597 (2012).
11. F. Wang, Y. Cai, H. T. Eyyuboglu, and Y. Baykal, "Twist phase-induced reduction in scintillation of a partially coherent beam in turbulent atmosphere," Opt. Lett. **37**(2), 184–186 (2012).
12. F. Gori and M. Santarsiero, "Devising genuine spatial correlation functions," Opt. Lett. **32**(24), 3531–3533 (2007).
13. F. Gori, V. Ramírez-Sánchez, M. Santarsiero, and T. Shirai, "On genuine cross-spectral density matrices," J. Opt. A: Pure Appl. Opt. **11**(8), 085706 (2009).
14. H. Lajunen and T. Saastamoinen, "Propagation characteristics of partially coherent beams with spatially varying correlations," Opt. Lett. **36**(20), 4104–4106 (2011).
15. J. Yu, Y. Cai, and G. Gbur, "Rectangular Hermite non-uniformly correlated beams and its propagation properties," Opt. Express **26**(21), 27894–27906 (2018).
16. Y. Chen, J. Gu, F. Wang, and Y. Cai, "Self-splitting properties of a Hermite-Gaussian correlated Schell-model beam," Phys. Rev. A **91**(1), 013823 (2015).
17. Z. Mei and O. Korotkova, "Random sources generating ring-shaped beams," Opt. Lett. **38**(2), 91–93 (2013).
18. J. Yu, F. Wang, L. Liu, Y. Cai, and G. Gbur, "Propagation properties of Hermite non-uniformly correlated beams in turbulence," Opt. Express **26**(13), 16333–16343 (2018).
19. Y. Gu and G. Gbur, "Scintillation of nonuniformly correlated beams in atmospheric turbulence," Opt. Lett. **38**(9), 1395–1397 (2013).
20. J. Yu, X. Zhu, F. Wang, D. Wei, G. Gbur, and Y. Cai, "Experimental study of reducing beam wander by modulating the coherence structure of structured light beams," Opt. Lett. **44**(17), 4371–4374 (2019).
21. G. Gbur, "Partially coherent beam propagation in atmospheric turbulence," J. Opt. Soc. Am. A **31**(9), 2038–2045 (2014).
22. Y. Cai, Y. Chen, and F. Wang, "Generation and propagation of partially coherent beams with nonconventional correlation functions: a review," J. Opt. Soc. Am. A **31**(9), 2083–2096 (2014).
23. Z. Mei and O. Korotkova, "Random sources for rotating spectral densities," Opt. Lett. **42**(2), 255–258 (2017).
24. L. C. Andrews and R. L. Phillips, *Laser Beam Propagation through Random Media* (SPIE, 2005).
25. S. M. Kim and G. Gbur, "Angular momentum conservation in partially coherent wave fields," Phys. Rev. A **86**(4), 043814 (2012).
26. G. Gbur, "Partially coherent vortex beams," Proc. SPIE **10549**, 2 (2018).
27. G. Gbur, *Singular optics* (CRC, Boca Raton 2016).
28. J. Yu, Y. Chen, L. Liu, X. Liu, and Y. Cai, "Splitting and combining properties of an elegant Hermite-Gaussian correlated Schell-model beam in Kolmogorov and non-Kolmogorov turbulence," Opt. Express **23**(10), 13467–13481 (2015).